AB

to be published in Phys. Lett. B

Preprint Bern BUHE-97-05

Baryon and antibaryon production in lead-lead collisions at 158 A GeV/c

Newmass (NA52) Collaboration

G. Ambrosini [a], R. Arsenescu [a], C. Baglin [c], J. Beringer [a], C. Bohm [e], K. Borer [a], A. Bussière [c], F. Dittus [a,1], K. Elsener [b], D. Frei [a], Ph. Gorodetzky [f], J. P. Guillaud [c], P. Hess [a], E. Hugentobler [a], S. Kabana [a], R. Klingenberg [a], T. Lindén [d], K. D. Lohmann [b], R. Mommsen [a], U. Moser [a], T. Pal [a], K. Pretzl [a], J. Schacher [a], B. Selldén [e], F. Stoffel [a], J. Tuominiemi [d], M. Weber [a], Q. P. Zhang [e]

[a] *Lab. for High Energy Physics, University of Bern, Sidlerstr. 5, CH-3012 Bern, Switzerland*

[b] *CERN, SL Division, CH-1211 Geneva 23, Switzerland*

[c] *CNRS-IN2P3, LAPP Annecy, F-74941 Annecy-le-Vieux, France*

[d] *Dept. of Physics, University of Helsinki, PO Box 9, FIN-00014 Helsinki, Finland*

[e] *Dept. of Physics, University of Stockholm, PO Box 6730, S-11385 Stockholm, Sweden*

[f] *CNRS-IN2P3, CRN Strasbourg, F-67037 Strasbourg, France*

We report on baryon and antibaryon as well as K^+ and K^- production cross sections measured in lead-lead collisions at 158 GeV/c per nucleon. The presented data were taken at zero degree production angle with a minimum bias trigger. The measurements covered a wide range of rapidity $1.4 < y < 6.0$. Using a simple thermodynamical and a coalescence model the temperature and the chemical potential of the particle source as well as the freeze-out radius of baryons and antibaryons have been deduced.

Key words:
PACS: 25.75.+r

[1] now at CERN, PPE Division, CH-1211 Geneva 23, Switzerland

1 Introduction

Baryon and antibaryon production measurements in heavy ion collisions provide information on the space time evolution of the high density state formed in the collision [1]. For instance, enhanced production of antinuclei was predicted in the event of a quark gluon plasma (QGP) formation [2–5]. Some models assume that baryons (antibaryons) arise via coalescence of three quarks (antiquarks) and are therefore sensitive to the thermal quark (antiquark) distributions and the chemically equilibrated abundances in the high density state. It was conjectured, that if a QGP was formed, the high density of antiquarks in the plasma may lead to an enhanced production of antibaryons. However, baryon-antibaryon annihilations in the baryon dense hadron gas may considerably dilute those abundances [6]. It is therefore of interest to measure and compare baryon and antibaryon production in heavy ion collisions in the BNL and CERN energy domain, where different energy and baryon densities can be reached.

Considering thermodynamical models, which assume the interaction volume to be in thermal and chemical equilibrium, particle production is mainly governed by the chemical potential and the temperature of the particle source at freeze out [7–9]. Therefore within this approach the temperature of the particle source as well as the chemical potential can be determined from the particle production cross section measurements. Another very basic parameter in heavy ion collisions is the size of the interaction volume, or the so called source size. So far the source size has been extensively studied by using pion or kaon interferometry [10,11] or proton-proton correlations [12,13]. Complementary information on the source size can be obtained from the production of light nuclei within the context of simple coalescence models [14–16]. The coalescence model implies that nucleons in the interaction volume which have a small relative momentum $\tilde{p}_0$ will coalesce to produce a cluster. As the volume of the fireball expands the composite particles will cease from colliding with other particles and freeze out. The models [15,16] relate the relative momentum to the interaction volume. Thus, within the framework of these models the source size can be deduced from the inclusive composite particle cross sections. It is important to measure and carefully analyse these parameters as a function of the energy density in order to observe variations, which could signalize a phase transition from a hadronic gas to a QGP.

Production rates of baryons and antibaryons have previously been studied at BNL [12,17–26] using silicon and gold beams of 14.6 A GeV/c and 11.4 A GeV/c, respectively, and at CERN [27–30] with sulfur beams of 200 A GeV/c and with lead beams of 158 A GeV/c [11].

In this paper we report on baryon and antibaryon as well as K^+ and K^-

production cross sections obtained with the NA52 experiment in lead-lead collisions. The data were obtained in a few days of running time which were specially devoted to the measurement of the particle yields, since the main goal of the NA52 experiment was the search for strangelets in lead-lead collisions [32]. The analysis of the data on pion production, recorded during the same run, is in progress.

2 Experimental set up

The experimental set up is shown in Fig. 1. The experimental method is described in more detail in ref. [31,33]. The secondary beam line H6 in the North Area of the SPS at CERN was used as a spectrometer. Its momentum and solid angle acceptance were 2.8 % and 2.2 μsr, respectively. The incident lead ions were counted in a segmented, 0.4 mm thick quartz Čerenkov counter (TOF0). The average lead beam intensity was 10^8 ions per spill with a spill duration of 5 seconds. The spectrometer was aligned at zero degree with respect to the incident ion beam. Two different targets were used: either a lead target of 4 mm thickness in TL1 or a 40 mm thick lead target in TL2. The mass to charge ratio m/Z of the produced particles was determined through the spectrometer rigidity (p/Z) and the velocity measurement with the time of flight (TOF) detectors (TOF0-TOF5). The individual time resolutions of the TOF detectors varied between σ = 74-105 ps. Additional particle identification capabilities were provided by one differential (CEDAR) and three threshold (Č0, Č1 and Č2) Čerenkov counters. The Čerenkov counters were especially useful at high rigidities ($>$ 40 GeV/c) where the TOF measurements were not sufficient to separate the particles. The charge of the particles was measured by their energy loss (dE/dx) in the TOF1-5 counters. A segmented scintillator/uranium calorimeter at the downstream end of the spectrometer added further particle identification capabilities and redundancy to the charge measurements. Seven sets of multiwire proportional chambers (W1T-W5T, W2S, W3S) were used for particle tracking.

3 Data samples

Data were taken at spectrometer rigidities $p/Z = \pm5$, ±10, ±20, ±40, ±100 and ±200 GeV/c. Most of the statistics was collected at the rigidities of ±100 and ±200 GeV/c, which were the spectrometer settings for the strangelet search. At low rigidites ($<$ 100 GeV/c) the data were taken with a 4 mm thick lead target, while at high rigidities (±100 GeV/c, -200 GeV/c) a 40 mm and at $+200$ GeV/c a 16 mm thick lead target were used. Empty target runs were

performed at the rigidities ± 10, ± 20, -40, $+200\,\mathrm{GeV}/c$, in order to evaluate the background due to interactions in the air and in the materials in the T4 target box.

In all cases the detector information satisfying a coincidence between TOF2 and B1 was recorded. We restricted the analysis of the low rigidity data to particles reaching at least TOF3. At high rigidities the information of the CEDAR and Č2 Čerenkov counters were necessary for particle identification and therefore particles were required to reach TOF5. Typical mass distributions of particles obtained at low and high rigidities with the TOF system are shown in ref. [31]. Examples of the particle identification capability of the combined TOF and Čerenkov counter system are also presented in that reference.

The results shown here contain the full data sample taken in the 1994 and 1995 running periods.

4 Results

The invariant differential production cross section for particles with the energy E and the momentum p was evaluated from

$$E\frac{d^3\sigma}{dp^3} = \frac{N_s}{N_i}\cdot\frac{\eta}{\epsilon}\cdot\frac{1}{n\cdot\alpha}\cdot\frac{E}{p^3} \qquad (1)$$

with N_s, the number of observed secondary particles, N_i, the number of incident lead ions, n, the number of target nuclei per unit area, and α, the spectrometer acceptance. The factor ϵ accounts for the absorption of the incident ions and the secondary particles in the production target. It also takes into account the absorption and the lifetime of the secondaries in the spectrometer as well as the trigger and reconstruction efficiencies. The spectrometer acceptance α was deduced from the comparison of the measured beam profiles with a Monte Carlo simulation using the program DECAY TURTLE [34] which takes multiple scattering into account. In the Monte Carlo simulations a flat momentum distribution over the angular acceptance of the spectrometer was assumed. By comparing the Monte Carlo simulated and the experimentally obtained beam profiles, discrepancies of the spectrometer acceptance of 30 % for the high rigidities ($\pm 100, \pm 200\,\mathrm{GeV}/c$) and of 25 % for the lower rigidities were found. These discrepancies could not be resolved, consequently the mean value between the experimental and the simulated acceptance has been used with the corresponding error in the evluation of the production cross sections.

The empty target contributions to the particle yields turned out to be approximately the same for all particles and rigidities. Therefore, an empty target correction factor $\eta = 0.625$ with a systematic error of ± 0.05 was used to calculate the particle production cross sections. Pile up effects due to the spill structure of the extracted ion beam contributed $\approx 1\,\%$ to the overall systematic error. We estimated a total systematic error for the production cross section of 15 %, which is dominated by the uncertainty of the acceptance.

The obtained invariant production cross sections for positively (negatively) charged particles are summarized in Table 1 (2) and illustrated in Fig. 2 (3). Only the statistical errors are shown. It should be noted that no centrality cut has been applied to the data and no corrections for secondary interactions in the target were made. Some of the data at negative rigidities ($p/Z = -10$, -20, -100, $-200\,\mathrm{GeV}/c$) have already been published by this collaboration in a previous paper [31]. The cross sections quoted in this paper include small corrections as a result of a more refined acceptance determination and of a higher statistic collected in the 1995 running period (at -20 and $-200\,\mathrm{GeV}/c$).

In Fig. 4 the antiparticle to particle ratios as a function of the rapidity are also shown.

5 Discussion

Looking at the interaction volume V as a thermally and chemically equilibrated particle source, the inclusive particle production cross section, using Boltzmann statistics, can be written as

$$E\frac{d^3\sigma}{dp^3} = \sigma_{inel.} \cdot E \cdot \frac{2S+1}{(2\pi\hbar)^3} \cdot V \cdot \exp - \left(\frac{E-\mu_b}{kT}\right) \qquad (2)$$

with $\sigma_{inel.}$, the inelastic nucleus nucleus cross section, S, the spin of the particle, and μ_b the chemical potential. From the particle/antiparticle cross section ratios at central rapidity the ratio μ/kT can be evaluated

$$E_A\frac{d^3\sigma_A}{dp_A^3} \Big/ E_{\bar{A}}\frac{d^3\sigma_{\bar{A}}}{dp_{\bar{A}}^3} = \exp\left(\frac{2A\mu_b}{kT}\right) \qquad (3)$$

where A denotes the mass of the particle and $\bar{A}$ the mass of the corresponding antiparticle. We assume that $\mu_{\bar{A}} = -\mu_A = -A\mu_b$. The derived μ_b/kT ratios are listed in Table 3. Similarily using the K^+/K^- ratios near midrapidity we extracted values for μ_s/kT (with μ_s the strangeness chemical potential), which are also listed in Table 3.

From the cross section ratios of particles A/A' the source temperature kT can be derived using the weighted mean of the ratio $\langle \mu_b/kT \rangle = 1.118 \pm 0.034$ obtained from the cross section ratios $p/\overline{p}$ and $d/\overline{d}$ in Table 3. In this simple approach the effects of the different source sizes for different particles have been neglected, since their contributions are small. When using Fermi- and Bose-Einstein- instead of Boltzmann-statistics the results change by less than 1 %. The derived particle source temperatures and the baryo-chemical potentials are listed in Table 4. The evaluation of the source temperature comes out to be approximately 120 MeV when proton and antiproton cross sections are used. This appears to be rather low when compared to the temperatures (135-140 MeV) obtained from the d, $\overline{d}$ and t cross section ratios. However, possible contributions to the proton (antiproton) yield from the decay of higher lying resonances affect the temperature determination. In our analysis contributions of this kind have not been considered. Using VENUS [35] Monte Carlo simulations we estimated feeding contributions from Λ and Δ decays within our spectrometer acceptance. Feeding corrections for protons coming from these resonances would enhance the temperature to about 140 MeV, being consistent with the values determined from d/t ratios.

It is interesting to note that similar results were obtained when applying the Hagedorn model to our data [36]. Nevertheless our values of the source temperature are somewhat lower than the ones (160-170 MeV) obtained from an analysis of the sulfur-nucleus data in ref. [7] and lead-lead data in ref. [37]. This is not necessarily a contradiction since our results were derived from minimum bias events while in the analysis of ref. [7,37] only central collisions were considered.

Comparing thermodynamical parameters deduced from minimum bias and central events one has to keep in mind that the particle ratios may change with impact parameter. Similarily, when extracting particle source sizes, as described in the next paragraph, it is important to know that it was found to be strongly dependent on the centrality of the events [20]. The results of ref. [20] imply that the coalescence of nucleons into clusters is strongly influenced by the collision dynamics. Since this dependence has not been studied in lead-lead collisions at high energies our analysis of minimum bias data is a first step. We will study this question in more detail in a forthcoming data run where we will employ a lead/quartz-fibre calorimeter for a centrality measurement.

In order to extract the particle source size from our data the coalescence model developed by Sato and Yazaki [16] has been used. The model assumes that the highly exited region formed in the collision decays via particle emission. The momentum distribution of the particles within that region as well as the emitted composite particles are described by density matrices. The production yields of composite particles with respect to the nucleon production yields are related to the internal wavefunction parameter ν_A of the composite particle A

and the source size parameter ν

$$E_A \frac{d^3\sigma_A}{dp_A^3} \Big/ E_p \frac{d^3\sigma_p}{dp_p^3} \quad \propto \quad \left(\frac{\hbar}{m_N c^2}\right)^{A-1} \left(4\pi \frac{\nu_A \nu}{\nu_A + \nu}\right)^{\frac{3}{2}(A-1)} \tag{4}$$

where the rms source size radius is $R = \sqrt{3/(2\nu)}$. In this analysis the wave function parameters $\nu_d = 0.20\,\mathrm{fm}^{-2}$, $\nu_t = \nu_{^3\mathrm{He}} = 0.36\,\mathrm{fm}^{-2}$ from ref. [16] have been taken into account. The derived source sizes for nuclei and antinuclei are listed in Table 5. Also shown in Table 5 is the source size of deutrons in sulfur-tungsten collisions at 200 GeV/c per nucleon as derived from deuterium and proton yield measurements in an early run of the NA52 experiment [38]. While in sulfur-tungsten collisions the deuterium source size comes out to be comparable with the projectile radius (3.3 fm), the corresponding source size in lead-lead collisions turns out to be larger than the radius of the colliding projectiles (5.5 fm). This indicates that in lead-lead collisions the interaction volume is expanding before particle freeze out occurs. The source sizes for particles and antiparticles are found to be the same within the errors. It is interesting to note that the source size values obtained with this analysis are in qualitatively good agreement with the ones obtained in pion and kaon interferometry analysis (7-8 fm) of central lead-lead collisions [10,11].

6 Conclusion

For the first time baryon and antibaryon as well as K^+ and K^- production cross sections were measured in minimum bias lead-lead collisions at zero degree production angle. The measurements were performed at an incident energy of 158 GeV/c per nucleon covering a wide range of rapidity $1.4 < y < 6.0$. The chemical potentials for strangeness and baryons as well as the size and the temperature of the particle source were determined using a simple thermodynamical model. The temperature was found to be below the temperature (150-200 MeV) expected for a QGP phase transition. Furthermore the source size for the composite particles and antiparticles was derived from a coalescence model of Sato and Yazaki [16]. The source radius in lead-lead collisions turned out to be the same for particles and antiparticles and to be larger than the projectile radius indicating, that the interaction volume is expanding before the particles freeze out. This analysis is complementary to the source size determination using meson interferometry [10,11] or proton-proton correlations [12,13].

Acknowledgements

We are gratefull to H. Stöcker for valuable discussions. The enthusiastic support by the SPS operation team, the SL experimental areas and beam instrumentation groups and the SPS coordinator at CERN are greatly acknowledged. The experiment was supported by the Swiss National Foundation.

References

[1] U. Heinz et al., J. Phys. G12 (1986) 1237

[2] J. Ellis et al., Phys. Lett. B233 (1989) 223

[3] S. Gavin et al., Phys. Lett. B234 (1990) 175

[4] J. Schaffner et al., Z. Phys. A341 (1991) 47

[5] H. Sorge et al., Phys. Lett. B289 (1992) 6

[6] A. Jahns et al., Phys. Rev. Lett. 68, 19 (1992) 2895
St. Mrowczynski, Phys. Lett. B308 (1993) 216
M. Bleicher et al., Phys. Lett. B361 (1995) 10

[7] P. Braun-Munzinger et al., Phys. Lett. B365 (1996) 1

[8] J. Cleymans and H. Satz, Z. Phys. C57 (1993) 135-147

[9] J. Letessier et al., Phys. Rev. D51 (1995) 3408

[10] see Proceedings of the Quark Matter 1995, Nucl. Phys. A590 (1995)

[11] see Proceedings of the Quark Matter 1996, Nucl. Phys. A610 (1996)

[12] G. S. F. Stephans et al., Nucl. Phys. A566 (1994) 269c

[13] J. Barrette et al., Nucl. Phys. A610 (1996) 227c

[14] S. T. Butler and C. A. Pearson, Phys. Rev. 129, 2 (1963) 836-842
A. Schwarzschild and Č. Zupančič, Phys. Rev. 129, 2 (1963) 854

[15] A. Z. Mekjian, Phys. Rev. Lett. 38 (1977) 640

[16] H. Sato and K. Yazaki, Phys. Lett. 98B (1981) 153

[17] T. Abbott et al., Phys. Lett. B 271 (1991) 447

[18] M. Aioki et al., Phys. Rev. Lett. 69 (1992) 2345

[19] J. Barrette et al., Phys. Rev. Lett. 70 (1993) 1763

[20] J. Barrette et al., Phys. Rev. C50, 2 (1994) 1077

[21] N. Saito et al., Phys. Rev. C49, 6 (1994) 3211

[22] G. E. Diebold et al., Phys. Rev. C48 (1993) 2984

[23] D. Beavis et al., Phys. Rev. Lett. 75 (1995) 3633

[24] M. J. Bennett et al., Nucl. Phys. A590 (1995) 491c

[25] B. S. Kumar et al., Nucl. Phys. A566 (1995) 439c

[26] P. Stankus et al., Nucl. Phys. A544 (1992) 603c

[27] J. Dodd et al., Nucl. Phys. A590 (1995) 523c

[28] J. Simmon-Gillo et al., Nucl. Phys. A590 (1995) 483c

[29] J. Günther et al., Nucl. Phys. A590 (1995) 487c

[30] T. Alper et al., Phys. Lett. B366 (1996) 56

[31] G. Appelquist et al., Phys. Lett. B376 (1996) 245

[32] G. Appelquist et al., Phys. Rev. Lett. 76 (1996) 3907

[33] K. Pretzl et al., Proceedings of the International Symposium on Strange and Quark Matter (Crete Hellas Sept. 1994), ed. by G. Vassiliadis, A. D. Panagiotou, B. S. Kumar and J. Madsen, World Scientific (1995) 230

[34] K. L. Brown and C. Iselin, Decay Turtle, CERN rep. CERN-74-2 (1974)

[35] VENUS 4.12, see K. Werner, Phys. Rep. 232 (1993) 87

[36] P. Sonderegger et al., in Critical Phenomena and Collective Observables CRIS 96, World Scientific (1996) 225

[37] J. Stachel, Nucl. Phys. A610 (1996) 509c-522c

[38] K. Borer et al., Phys. Rev. Lett. 72, 10 (1994) 1415
Q. P. Zhang et al., Proceedings of the International Symposium on Strange and Quark Matter (Crete Hellas Sept. 1994) ed. by G. Vassiliadis, A. D. Panagiotou, B. S. Kumar and J. Madsen, World Scientific (1995) 276

Table 1
Invariant differential particle production cross sections with statistical errors. The systematic errors are 15 % for all rigidities. The particles were not selected for central collisions.

Particle	Rigidity $[\mathrm{GeV}/c]$	Rapidity y	Cross section $\left[\frac{\mathrm{barn}}{\mathrm{GeV}^2}c^3\right]$
K^+	+5	3.01	39.9 ± 12.1
	+10	3.70	32.5 ± 2.7
	+20	4.40	33.89 ± 0.88
	+40	5.09	21.4 ± 1.3
p	+5	2.38	21.14 ± 0.93
	+10	3.06	24.52 ± 0.86
	+20	3.75	30.64 ± 0.75
	+40	4.45	45.6 ± 1.2
d	+5	1.71	0.182 ± 0.031
	+10	2.38	$(9.77 \pm 0.81) \cdot 10^{-2}$
	+20	3.06	$(8.91 \pm 0.42) \cdot 10^{-2}$
	+40	3.75	0.1663 ± 0.0061
	+100	4.67	0.633 ± 0.023
	+200	5.36	5.30 ± 0.01
^{3}He	+5	1.98	$(12 \pm 12) \cdot 10^{-4}$
	+10	2.66	$(1.6 \pm 1.6) \cdot 10^{-4}$
	+20	3.35	$(1.84 \pm 0.76) \cdot 10^{-4}$
	+40	4.04	$(15.0 \pm 1.9) \cdot 10^{-4}$
	+200	5.65	5.27 ± 0.01
t	+5	1.34	$(51 \pm 51) \cdot 10^{-4}$
	+10	1.98	$(6.5 \pm 6.5) \cdot 10^{-4}$
	+20	2.66	$(2.4 \pm 1.7) \cdot 10^{-4}$
	+40	3.35	$(5.4 \pm 2.2) \cdot 10^{-4}$

Table 2
As Table 1 for antiparticle production.

Particle	Rigidity $[\mathrm{GeV}/c]$	Rapidity y	Cross section $\left[\frac{\mathrm{barn}}{\mathrm{GeV}^2 c^3}\right]$
K^-	-5	3.01	13.2 ± 4.6
	-10	3.70	20.5 ± 1.4
	-20	4.40	15.79 ± 0.51
	-40	5.09	7.30 ± 0.25
$\overline{\mathrm{p}}$	-5	2.38	2.08 ± 0.12
	-10	3.06	2.690 ± 0.095
	-20	3.75	1.993 ± 0.054
	-40	4.45	0.578 ± 0.032
	-100	5.36	$(7.9 \pm 0.2) \cdot 10^{-4}$
$\overline{\mathrm{d}}$	-5	1.71	$< 41.3 \cdot 10^{-4}$ (90% UL)
	-10	2.38	$(7.3 \pm 4.2) \cdot 10^{-4}$
	-20	3.06	$(8.0 \pm 1.3) \cdot 10^{-4}$
	-40	3.75	$(3.03 \pm 0.35) \cdot 10^{-4}$
	-100	4.67	$(29.0 \pm 3.4) \cdot 10^{-6}$
	-200	5.36	$(0.393 \pm 0.041) \cdot 10^{-6}$
$^3\overline{\mathrm{He}}$	-20	3.35	$(4.6 \pm 4.6) \cdot 10^{-6}$

Table 3
$\mu_b/(kT)$ and $\mu_s/(kT)$ ratios as derived from matter/antimatter production cross section ratios near central rapidity for minimum bias data.

	y	$\frac{\mu_b}{kT}$
$\mathrm{p}/\overline{\mathrm{p}}$	3.06	1.089 ± 0.043
$\mathrm{d}/\overline{\mathrm{d}}$	3.06	1.163 ± 0.055
	y	$\frac{\mu_s}{kT}$
$\mathrm{K}^+/\mathrm{K}^-$	3.01	0.55 ± 0.23
$\mathrm{K}^+/\mathrm{K}^-$	3.70	0.232 ± 0.053

Table 4
The temperatures and the baryochemical potential of the particle source for minimum bias data are shown.

	kT [MeV]	μ_b [MeV]
d/p	120.7 ± 1.8	134.9 ± 2.0
$\overline{\mathrm{d}}/\overline{\mathrm{p}}$	117.1 ± 3.1	130.9 ± 3.5
d/t	135.8 ± 9.3	152 ± 10
$\overline{\mathrm{d}}$/t	139.5 ± 4.9	155.9 ± 5.4

Table 5
The source size parameters R_{rms} using the coalescence model [16] for lead-lead collisions at 158 and sulfur-tungsten collisions at 200 GeV/c per nucleon are shown. The relative coalescence momentum $\tilde{p}_0$ [15] derived from the data are also listed.

Pb + Pb			
(anti) particle	A	$\tilde{p}_0$ [MeV]	R_{rms} [fm]
d	2	49.1 ± 4.2	7.15 ± 0.71
$\overline{\mathrm{d}}$	2	51.4 ± 5.2	6.79 ± 0.79
^{3}He	3	$64.7^{+5.6}_{-10.3}$	$6.70^{+1.38}_{-0.59}$
$^3\overline{\mathrm{He}}$	3	113^{+14}_{-113}	$3.44^{+\infty}_{-0.52}$
t	3	$63.0^{+6.9}_{-17.9}$	$6.90^{+2.95}_{-0.74}$
S + W			
particle	A	$\tilde{p}_0$ [MeV]	R_{rms} [fm]
d	2	100 ± 12	2.55 ± 0.64

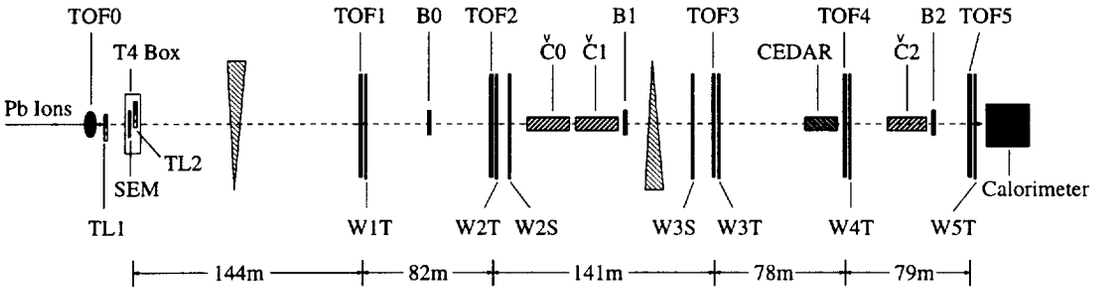

Fig. 1. The experimental set-up.

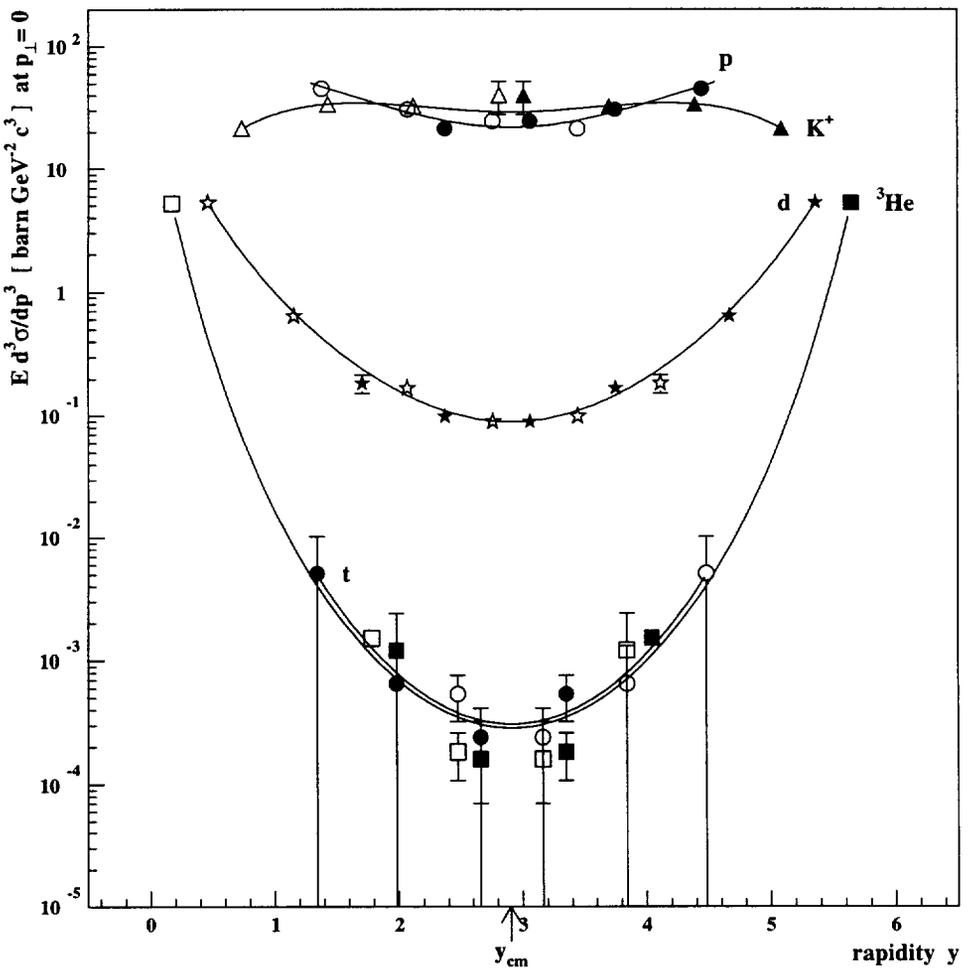

Fig. 2. Invariant differential particle production cross sections for minimum bias events as a function of rapidity (closed symbols). The open symbols are data points reflected at midrapidity (y_{cm} = 2.9). Only the statistical errors are shown. Lines are drawn to guide the eye.

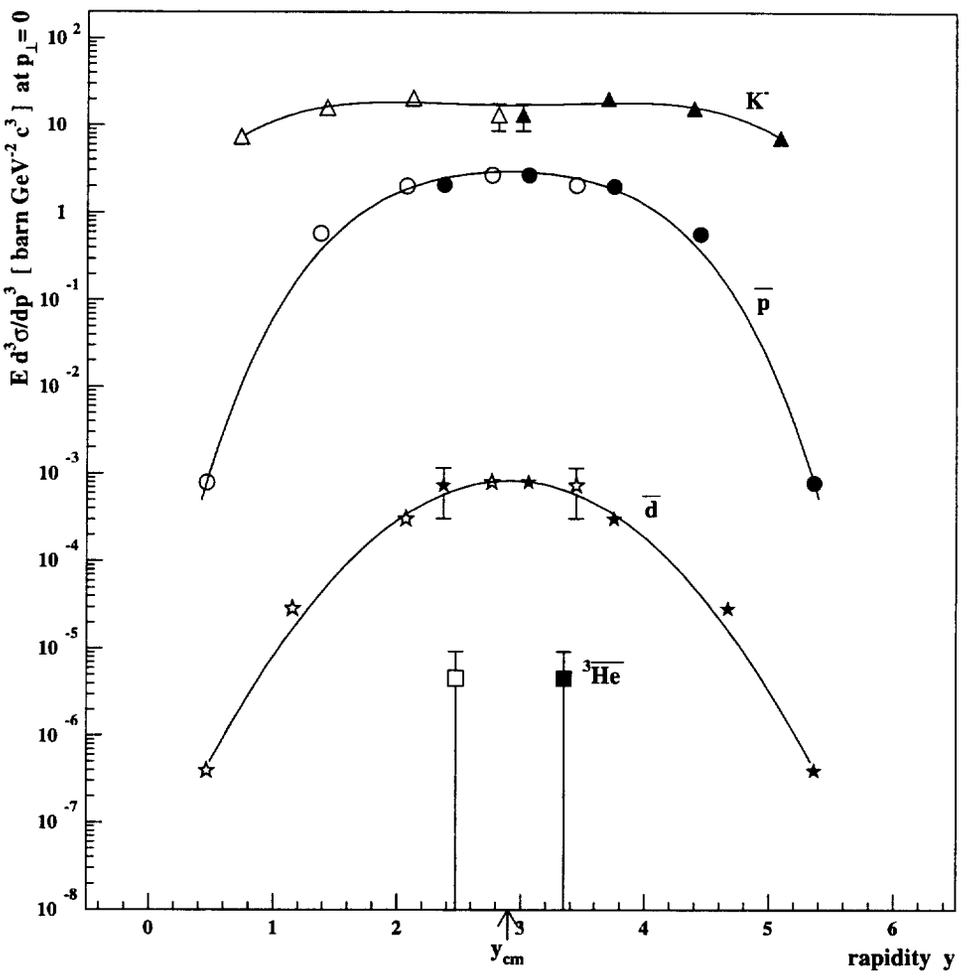

Fig. 3. As Fig. 2 for antiparticle production.

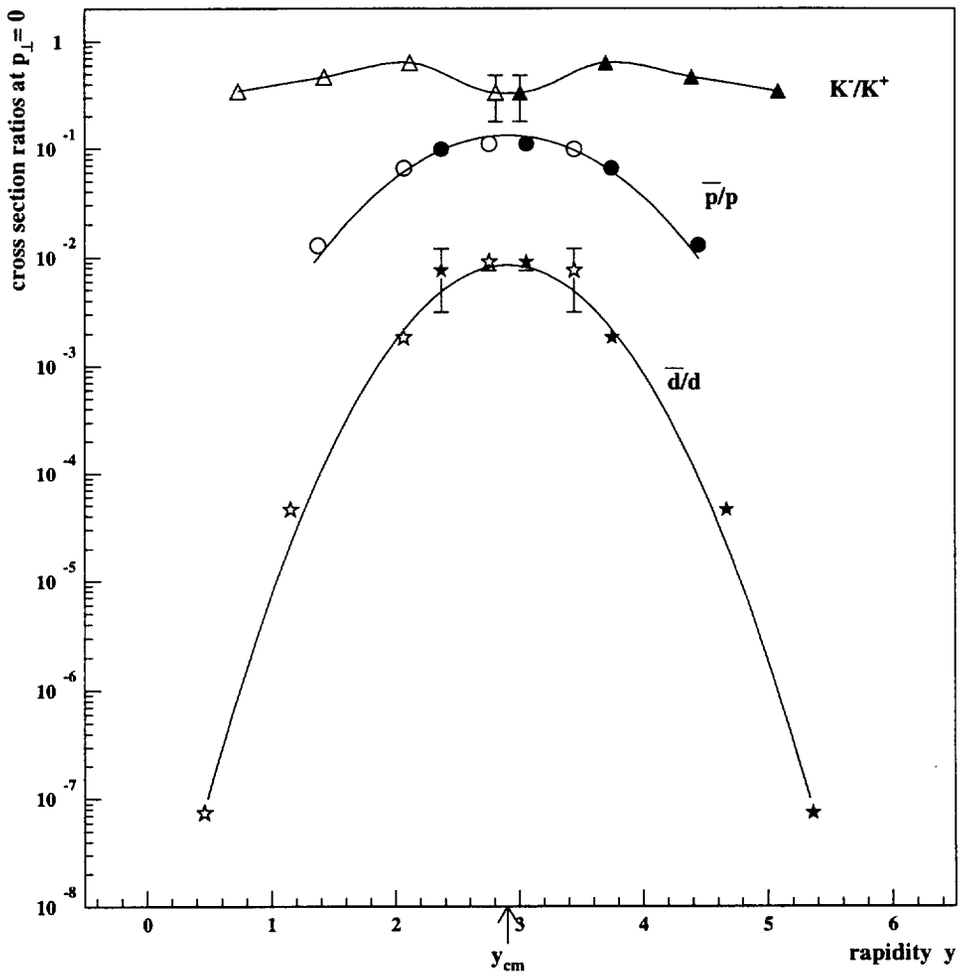

Fig. 4. The antiparticle to particle cross section ratios for minimum bias events are shown. The open symbols are data points reflected at midrapidity ($y_{cm} = 2.9$).